ISSN: 1410-8917
Jurnal Kimia Sains & Aplikasi
e-ISSN: 2597-9914

Jurnal Kimia Sains dan Aplikasi 28 (1) (2025): 31-38

Jurnal Kimia Sains dan Aplikasi
Journal of Scientific and Applied Chemistry

Journal homepage: http://ejournal.undip.ac.id/index.php/ksa

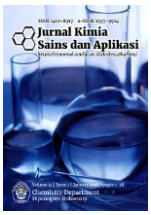

Synthesis of TiO_2/Hydroxyapatite Composite Based on Chicken Egg Shells for Methylene Blue Photodegradation

Dhea Annisa Zein [1,*], F. Widhi Mahatmanti [1], Sri Wahyuni [1], Nuni Widiarti [1]

[1] Department of Chemistry, Faculty of Sciences and Mathematics, Universitas Negeri Semarang, Semarang, Indonesia

* Corresponding author: dheaannisa65@students.unnes.ac.id

https://doi.org/10.14710/jksa.28.1.31-38

Article Info

Article history:

Received: 07th August 2024
Revised: 01st January 2025
Accepted: 08th January 2025
Online: 31st January 2025

Keywords:
hydroxyapatite; TiO_2; photodegradation; adsorption; methylene blue

Abstract

Hydroxyapatite (HAp) was synthesized using low-cost eggshell waste and employed as a composite support material for a TiO_2 photocatalyst. The TiO_2/HAp composite was characterized using X-ray diffraction (XRD), Fourier-transform infrared (FTIR) spectroscopy, and a surface area analyzer (SAA). XRD analysis confirmed the presence of TiO_2/HAp, revealing a crystallite size of 9.42 nm. The FTIR spectra further verified the characteristic peaks of TiO_2/HAp, corresponding to those of TiO_2 and HAp. BET-BJH analysis indicated that the surface area followed the trend TiO_2 > TiO_2/HAp > HAp trend, while the pore volume and diameter followed the HAp > TiO_2 > TiO_2/HAp. The photocatalytic activity of TiO_2/HAp in methylene blue degradation was evaluated using a UV-Vis spectrophotometer, demonstrating excellent performance. The TiO_2/HAp composite achieved a 99.10% photodegradation of 20 ppm methylene blue within 120 minutes, with an adsorption capacity of 8.3078 mg/g. The photodegradation efficiency for 40 ppm methylene blue was 86.47%, with an adsorption capacity of 13.6335 mg/g. These results confirm that HAp effectively inhibits the electron recombination process in TiO_2, thereby enhancing its photocatalytic performance. This study highlights the potential of HAp for developing cost-effective and high-efficiency TiO_2-based photocatalysts, offering a sustainable and environmentally friendly approach to water purification.

1. Introduction

One of the most significant environmental issues is pollution caused by dye contaminants in wastewater. The textile industry is the primary contributor to this pollution, accounting for 54% of the total [1] It is estimated that over 100,000 dyes are available on the market, with annual production volumes ranging from 7 × 10^5 to 1 × 10^6 tons [2]. Approximately 20% of these dyes dissolve in wastewater as a byproduct of textile manufacturing processes [3]. Methylene blue is one of the most widely used dyes, with applications across various industries [4]. However, exposure to methylene blue can cause permanent eye damage in both humans and animals. Due to its stability and non-degradable nature, methylene blue is considered a major pollutant in wastewater [5].

Various technological methods have been developed to address water pollution, including chlorination, biodegradation, and ozonation. However, these methods are often less effective in treating dye wastewater and may lead to secondary environmental issues [6]. In contrast, photocatalytic methods offer an efficient solution by degrading pollutants rapidly without generating secondary pollution.

The photocatalytic process involves the excitation of semiconductor materials with an energy source greater than the band gap of the semiconductor photocatalyst. Once the electron-hole pairs are excited, they can either recombine or react with the target substance, resulting in the formation of electron acceptors (e.g., molecular oxygen) or electron donors (e.g., hydroxide ions) [7]. During photodegradation, highly reactive species such as superoxide and hydroxyl radicals are generated [8]. These free radicals then attack dye molecules in wastewater, breaking them down into smaller, environmentally harmless compounds such as CO_2 and H_2O [9].

Among various semiconductor photocatalysts, TiO_2 has garnered significant attention due to its stability, non-toxicity, ease of synthesis, and cost-effectiveness [10, 11, 12]. When irradiated by a light source, electron-hole pairs form on the surface of TiO_2, which can either recombine—producing thermal energy—or generate hydroxyl radicals that facilitate the breakdown of dye pollutants into simpler compounds [7]. However, TiO_2 suffers from a high electron-hole recombination rate, which reduces its photocatalytic efficiency [9]. To overcome this limitation, supporting materials are required to enhance its photocatalytic performance.

Hydroxyapatite (HAp, $Ca_{10}(PO_4)_6(OH)_2$) is a promising supporting material that can aid TiO_2 in inhibiting electron-hole recombination [9]. Under UV irradiation, PO_4^{2-} groups on the surface of HAp create oxygen vacancies, leading to the formation of superoxide radicals (O_2^-) [9]. Consequently, hydroxyapatite exhibits photoinductive activity and the ability to degrade persistent dyes.

Compositing hydroxyapatite with TiO_2 serves as an effective strategy to suppress electron-hole recombination in TiO_2, thereby enhancing its photocatalytic performance in decomposing organic compounds under UV irradiation [9]. In this study, hydroxyapatite was derived from chicken eggshells, a widely available waste material. The primary components of hydroxyapatite are calcium and phosphate, and eggshells contain 94–97% calcium carbonate ($CaCO_3$). Approximately 7.2 million tons of eggshell waste are generated annually [13, 14]. Utilizing eggshell waste as a raw material for hydroxyapatite production not only reduces environmental pollution but also lowers production costs.

Singh *et al.* [15] synthesized TiO_2/hydroxyapatite composites using goat bone as a precursor via the sol-gel method for methylene blue degradation. The photocatalytic degradation process was conducted under a 12 W UV light source with a methylene blue concentration of 20 M. The photodegradation test was repeated 10 times, yielding an efficiency of 92.9%.

Similarly, Echabbi *et al.* [16] investigated TiO_2/hydroxyapatite composites derived from oyster shells for methylene blue degradation. Photodegradation tests were performed using six 8 W UV lamps (three UV-A and three UV-B). The study varied the methylene blue concentration at 10, 20, and 30 mg/L, achieving degradation efficiencies of 97, 90, and 57%, respectively. Additionally, pH variations were tested at 3.2, 6.3, and 10.6, with the highest degradation kinetics observed under alkaline conditions (pH 10.6). Notably, oyster shells contain approximately 96% $CaCO_3$.

El Abbadi *et al.* [5] synthesized TiO_2/hydroxyapatite composites using bovine teeth, which contain 58.91% calcium as a precursor. Following a similar approach, photodegradation tests were conducted under six 8 W UV lamps (three UV-A and three UV-B). Methylene blue concentrations varied at 0.01, 0.02, and 0.03 g/L, resulting in 98, 87, and 82% degradation efficiencies, respectively. The study also examined pH variations at 2.0, 6.2, and 8.0, with maximum degradation kinetics observed at pH 8.0 (alkaline conditions).

This study aims to synthesize TiO_2 modified with HAp derived from chicken eggshells. The incorporation of HAp is intended to inhibit electron recombination in TiO_2 and enhance its photocatalytic performance. Additionally, this research attempts to investigate the effects of varying concentrations and activity testing durations on the performance of TiO_2/HAp composites.

2. Experimental

2.1. Materials and Instruments

The materials used in this study included eggshells, nitric acid (HNO_3) (Merck), potassium dihydrogen phosphate (KH_2PO_4) (Merck), ammonia (NH_3) (Merck), titanium dioxide (TiO_2) (Merck), methylene blue (Merck), and demineralized water (Water One). The instruments used for characterization and analysis included a UV-Visible spectrophotometer (FLUOstar Omega), X-ray diffraction (XRD) (Rigaku MiniFlex 600), Fourier-transform infrared (FTIR) spectrometer (Shimadzu 8300), and surface area analyzer (SAA) (Nova version 11.0).

2.2. Preparation and Characterization of Chicken Egg Shells

The chicken eggshell membrane was cleaned, boiled, and then dried in an oven at 105°C for 6 hours. The dried eggshells were ground using a blender and sieved through a 100-mesh sieve. Subsequently, they were calcined at 900°C for 2 hours to convert $CaCO_3$ in the eggshells into CaO [17]. The eggshells were characterized using XRD before and after calcination.

2.3. Synthesis of HAp

A total of 0.1 mol of CaO obtained from eggshell calcination was added to 100 mL of distilled water. Then, 0.2 mol of HNO_3 solution was added to dissolve CaO into $Ca(NO_3)_2$ under constant stirring at 60°C until the solution became clear. The resulting solution corresponded to 1 M $Ca(NO_3)_2$. A 0.6 M KH_2PO_4 solution was prepared using demineralized water, based on the stoichiometric ratio, ensuring that when reacted with 1 M $Ca(NO_3)_2$, a precipitate with a Ca/P molar ratio of 1.67 would be obtained. Simultaneously, a dilute NH_3 solution (3% v/v) was added slowly to maintain a pH of 10. The solution was stirred continuously for 1 hour and left at room temperature for 24 hours. The precipitate was washed until neutral pH was reached to remove K^+, NH_4^+, and NO_3^- ions. The sediment was then filtered, dried in an oven at 105°C for 6 hours, and calcined at 700°C for 30 minutes [17].

2.4. Synthesis of TiO_2/HAp Composite

Commercial TiO_2 was calcined at 500°C for 2 hours to obtain the anatase phase. The TiO_2/HAp composite was prepared by mixing calcined TiO_2 with HAp derived from chicken eggshells at a 1:1 mass ratio. The mixture was dissolved in 100 mL of demineralized water and stirred for 24 hours. It was then left undisturbed for 48 hours to allow precipitation. The precipitate was filtered using

Whatman No. 42 filter paper, dried in an oven at 105°C for 6 hours, and subsequently calcined at 500°C for 3 hours [18, 19].

2.5. Photocatalytic Activity Test of Methylene Blue Degradation

The photocatalytic activity of methylene blue degradation was evaluated using HAp, TiO_2, and TiO_2/HAp catalysts. The concentrations of methylene blue used were 20 ppm and 40 ppm, with 10 mL of each solution (0.25% catalyst per liter of solution). The photocatalytic activity test consisted of two stages: adsorption and photodegradation. In the first stage, the mixture was stirred in the dark for 30 minutes at 150 rpm to reach adsorption equilibrium on the catalyst surface. Subsequently, the photocatalytic test was conducted under UV irradiation for varying times: 30, 40, 60, 90, and 120 minutes, with stirring at 150 rpm. Samples were then centrifuged for 15 minutes at 2500 rpm. The concentration of degraded methylene blue and degradation efficiency were analyzed using a UV-Vis Spectrophotometer and calculated using Equations 1 and 2.

$$\text{Concentration of degraded methylene blue} = C_0 - C_t \quad (1)$$

$$\text{Degradation efficiency (\%)} = \left(\frac{C_0 - C_t}{C_0}\right) \times 100 \quad (2)$$

where C_0 is the absorbance (t = 0), and C_t is the absorbance at time *t*.

2.6. Photocatalyst Characterization

The HAp, TiO_2 catalyst materials, and TiO_2/HAp composites were characterized using XRD to determine the structure and crystallinity of the materials. FTIR analysis was conducted to identify the functional groups present in the catalyst materials. The pore structure was analyzed using the Brunauer-Emmett-Teller (BET) and Barrett-Joyner-Halenda (BJH) methods.

3. Results and Discussion

3.1. Synthesis and Characterization of Eggshell HAp

Eggshells contain $CaCO_3$, as evidenced by the diffraction pattern analysis in Figure 1. $CaCO_3$ is converted into CaO through a high-temperature calcination process, which induces a decomposition reaction. The heat energy breaks the chemical bonds in the sample, releasing CO_2 and forming CaO. The reaction during calcination is shown in Equation 3 [17]. The peaks produced by $CaCO_3$ derived from eggshells correspond to 2θ values of 13.08° (102), 29.46° (104), 36.05° (110), 39.48° (114), 43.23° (202), 47.57° (018), 48.58° (116), 57.71° (214), and 64.70° (300), as reported in the literature [20, 21, 22]. This indicates that the peak produced is from the $CaCO_3$ calcite phase. After calcination at 900°C, CaO forms, as confirmed by the XRD data. The corresponding peaks are at 2θ values of 18.1° (001), 28.58° (111), 29.27° (104), 34.10° (200), 39.25° (113), 47.15° (018), 50.72° (110), and 54.04° (220), in line with the literature [20, 23].

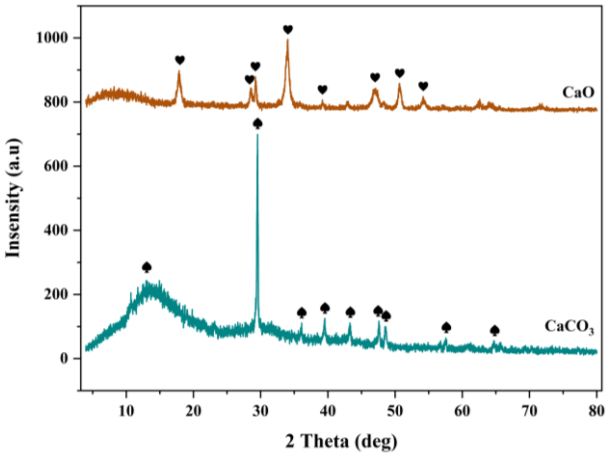

Figure 1. XRD patterns of $CaCO_3$ and CaO

The decomposition of $CaCO_3$ into calcium oxide (CaO) and CO_2 during the calcination process is represented by Equation 3 [17].

$$CaCO_{3(s)} \xrightarrow{\Delta} CaO_{(s)} + CO_{2(g)} \quad (3)$$

To produce a calcium hydroxide solution, the CaO obtained from the calcined eggshells is reacted with water, as shown in Equation 4 [17].

$$CaO_{(s)} + H_2O_{(l)} \rightarrow Ca(OH)_{2(l)} \quad (4)$$

The addition of nitric acid (HNO_3) serves to convert calcium hydroxide into the more soluble calcium nitrate ($Ca(NO_3)_2$), as described in Equation 5.

$$Ca(OH)_{2(l)} + 2HNO_{3(l)} \rightarrow Ca(NO_3)_{2(l)} + 2H_2O_{(l)} \quad (5)$$

HAp is synthesized under alkaline conditions, with the solution pH adjusted to 10 using dilute ammonia (NH_3). Maintaining a basic pH ensures a high concentration of hydroxide ions (OH^-), which promotes the formation of HAp. The chemical formula of HAp, $Ca_{10}(PO_4)_6(OH)_2$, indicates that OH^- ions play a crucial role in its synthesis. An acidic environment, on the other hand, favors the formation of alternative calcium phosphate phases such as monetite ($CaHPO_4$) and brushite ($CaHPO_4{\cdot}2H_2O$) [24]. The overall reaction for HAp synthesis is shown in Equation 6.

$$10Ca(NO_3)_{2(l)} + 6KH_2PO_{4(l)} + 14NH_4OH_{(l)} \rightarrow Ca_{10}(PO_4)_6(OH)_{2(s)} + 6K^+ + 4NH_4^+ + 20NO_3^- + 12H_2O_{(l)} \quad (6)$$

3.2. Characterization of TiO_2/HAp

3.2.1. X-ray Diffraction (XRD) Analysis

The diffraction patterns of HAp, TiO_2, and TiO_2/HAp were analyzed within a 2θ range of 5°–80°, as shown in Figure 2. The characteristic diffraction peaks of HAp were observed at 2θ values of 13.78° (100), 25.94° (002), 28.43° (102), and 30.78° (211), consistent with previous studies [14, 25]. For TiO_2 in the anatase phase, the diffraction peaks were located at 2θ values of 24.68° (101), 37.10° (004), 37.92° (112), 47.57° (200), 53.39° (202), 54.51° (211), 62.26° (204), 68.18° (116), 69.70° (220), and 74.60° (215), in line with the literature [25, 26].

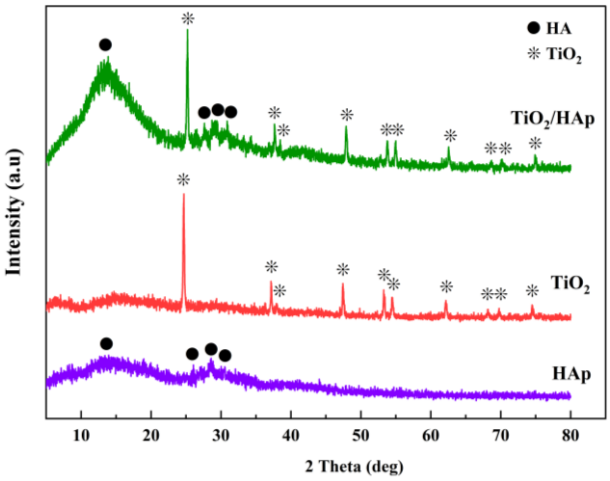

Figure 2. XRD patterns of HAp, TiO_2, and TiO_2/HAp

The crystallite size of a material can be calculated using the Debye-Scherrer equation (Equation 7).

$$D = \frac{k\lambda}{\beta cos\theta} \quad (7)$$

Where, D is the crystallite size, k = 0.9 is the Scherrer constant, λ = 0.154060 nm is the X-ray wavelength, β is the Full Width and Half Maximum (FWHM), and θ is the Bragg angle.

The crystallinity (X_c) of the sample is determined using Equation 8.

$$X_c = \frac{V_{002}}{I_{101}} \quad (8)$$

Where, V_{002} is the intensity of the (002) peak, and I_{101} is the highest intensity of the sample.

The calculated crystallite sizes for HAp, TiO_2, and TiO_2/HAp are 1.33 nm, 18.13 nm, and 9.42 nm, respectively. The TiO_2/HAp crystallite size is smaller than the 30 nm reported for TiO_2/HAp synthesized via reprecipitation from pure phosphate [18]. Smaller crystallite sizes lead to larger surface areas, enhancing catalytic activity [27]. TiO_2 has a crystallinity of 58%, while TiO_2/HAp has 45%, reflecting the more amorphous nature of HAp. The diffraction pattern of TiO_2/HAp shows a peak shift compared to TiO_2 and HAp, suggesting structural interactions between the components.

3.2.2. Fourier-Transform Infrared (FTIR) Analysis

The FTIR spectra of HAp, TiO_2, and TiO_2/HAp photocatalysts (4000–400 cm^{-1}) are shown in Figure 3. HAp exhibits characteristic absorption bands between 559 and 1087 cm^{-1}, confirming the apatite phase [14]. Specifically, the absorption bands associated with the PO_4^{3-} group appear at 1023 cm^{-1} (asymmetric stretching) and 544, 719, 972, and 1129 cm^{-1} (bending modes) [28]. A small peak at 1511 cm^{-1} corresponds to the asymmetric vibration of CO_3^{2-} [14, 17, 29]. The presence of CO_3^{2-} in HAp results from the reaction of CaO molecules with atmospheric CO_2, leading to the reformation of $CaCO_3$ during HAp synthesis. Additionally, small absorption peaks at 3617, 3739, and 3866 cm^{-1} indicate hydroxyl (–OH) vibrations [30]. Both OH^- and PO_4^{3-} functional groups in the FTIR spectrum confirm the successful formation of HAp from calcium and phosphate precursors.

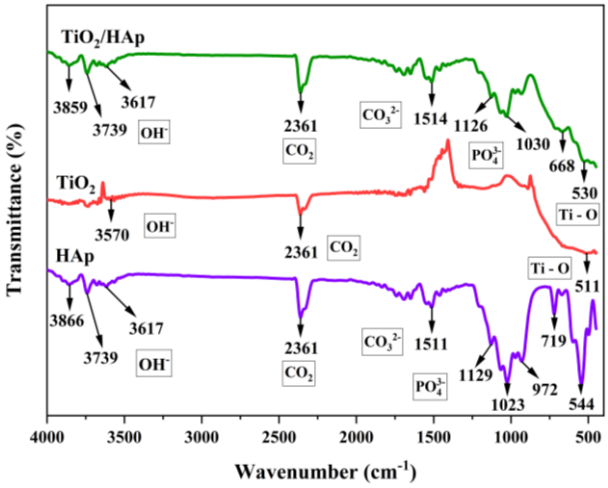

Figure 3. FTIR spectra of HAp, TiO_2, and TiO_2/HAp

The FTIR spectrum of TiO_2 displays an absorption band in the 500-600 cm^{-1} range, attributed to the stretching vibrations of the Ti–O bond. Furthermore, an absorption peak at 3570 cm^{-1} corresponds to –OH vibrations, which may arise from physically adsorbed water or Ti–O vibrations [31]. In the TiO_2/HAp composite spectrum, shifts in wave numbers indicate interactions between the composite components, such as hydrogen bonding between HAp and TiO_2. Additionally, an absorption peak at 2361 cm^{-1} suggests the presence of CO_2 clusters, likely originating from air contamination.

3.2.3. Surface Area Analyzer (SAA) Analysis

The BET method was used to determine the specific surface area and isotherm type of the materials, while the BJH method was employed to analyze the pore volume and pore diameter. Table 1 presents the pore distribution data for HAp, TiO_2, and TiO_2/HAp, while Figure 4 displays the N_2 adsorption-desorption isotherm curves.

Figure 4(a) shows the adsorption-desorption isotherm curve, which resembles a type IV isotherm according to IUPAC classification, indicating the presence of mesoporosity [15]. The BET surface area and pore volume of TiO_2 are 74.396 m^2/g and 0.1258 cm^3/g, respectively, while those of TiO_2/HAp are 52.489 m^2/g and 0.07862 cm^3/g, respectively. The decrease in surface area and pore volume of TiO_2/HAp compared to TiO_2 is attributed to pore blockage, a common phenomenon in supported catalysts [32]. Figure 4(b) presents the pore size distribution, showing 2–5 nm diameters.

Table 1. BET and BJH Pore Distribution for HAp, TiO_2, and TiO_2/HAp

Sample code	Surface area (m^2/g)	Pore volume (cc/g)	Pore diameter	
			(Å)	(nm)
HAp	33.14	0.09103	54.94	5.494
TiO_2	74.396	0.1258	33.81	3.381
TiO_2/HAp	52.489	0.07862	29.96	2.996

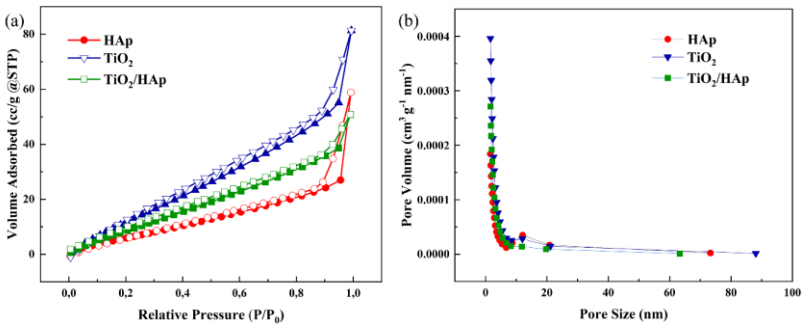

Figure 4. BET–BJH analysis curves for HAp, TiO_2, and TiO_2/HAp: (a) N_2 adsorption-desorption isotherm and (b) BJH adsorption pore size distribution curve

Table 2. Absorption capacity in the methylene blue adsorption process

Sample code	Q (mg/g)	
	20 ppm methylene blue	40 ppm methylene blue
HAp	4.5687	4.9921
TiO_2	0.5545	2.1485
TiO_2/HAp	0.5814	3.7915

3.3. Photocatalytic Studies

3.3.1. Adsorption and Photodegradation of Methylene Blue

The adsorption efficiency of methylene blue was evaluated under dark conditions for 30 minutes to ensure adsorption-desorption equilibrium on each photocatalyst. The adsorption and photodegradation efficiencies were calculated using Equation 9, where C_0 and C_t represent the initial concentration (ppm) of methylene blue and the concentration at time t, respectively.

$$D(\%) = \frac{(C_0 - C_t)}{C_0} \times 100 \quad (9)$$

The adsorption efficiencies of methylene blue on HAp, TiO_2, and TiO_2/HAp are presented in Figure 5. At an initial concentration of 20 ppm, the adsorption efficiencies were 58.47% (HAp), 7.13% (TiO_2), and 7.48% (TiO_2/HAp). At 40 ppm, the values were 31.66% (HAp), 13.62% (TiO_2), and 24.04% (TiO_2/HAp), respectively.

Figure 5 also illustrates the photodegradation efficiency of methylene blue under various stirring times (30, 40, 60, 90, and 120 minutes). The results show that UV irradiation time significantly affects the photodegradation process. Longer UV exposure increases the formation of hydroxyl radicals (-OH), thereby enhancing the degradation of methylene blue [6]. For instance, the photodegradation efficiency of TiO_2/HAp reached 99.10% at a methylene blue concentration of 20 ppm, but it decreased to 86.47% when the concentration was increased to 40 ppm.

Similar findings were observed by Safitri *et al.* [27]; they used $NiFe_2O_4$ to degrade methylene blue dye. At higher concentrations of methylene blue, more dye molecules adsorb onto the surface of the photocatalyst, which leads to the occupation of the active sites. As the irradiation time increases, the active sites become saturated with dye molecules, reaching an equilibrium point where no additional degradation occurs due to the blockage of active sites by the dye [14].

3.3.2. Absorption Capacity in the Adsorption and Photodegradation Process of Methylene Blue

The adsorption capacity (Q) represents the amount of substance (in milligrams) that can be adsorbed by each gram of adsorbent. It can be calculated using Equation 10, where C_0 and C_t are the initial and time-dependent concentrations of methylene blue (ppm), V is the solution volume (L), W is the catalyst mass (g), and Q is the adsorption capacity (mg/g).

$$Q = \frac{(C_0 - C_t) \times V}{W} \quad (10)$$

Table 2 presents the adsorption capacities of each catalyst for 20 ppm and 40 ppm of methylene blue after 30 minutes. At 20 ppm methylene blue, HAp exhibits a higher adsorption capacity compared to TiO_2 and TiO_2/HAp. This is because HAp has a larger pore diameter, which enhances its adsorption capacity relative to TiO_2 and TiO_2/HAp.

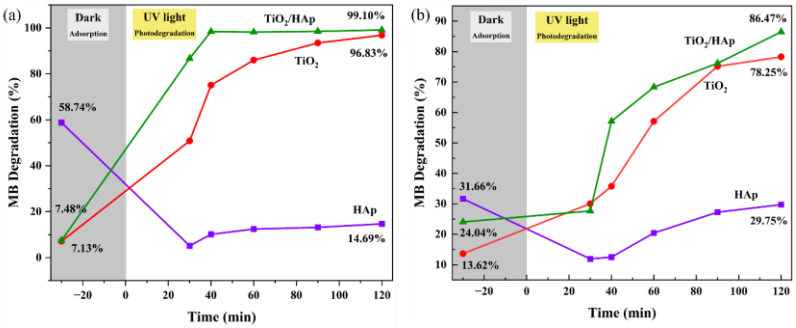

Figure 5. Adsorption and photodegradation efficiency curves of methylene blue at different concentrations: (a) 20 ppm and (b) 40 ppm

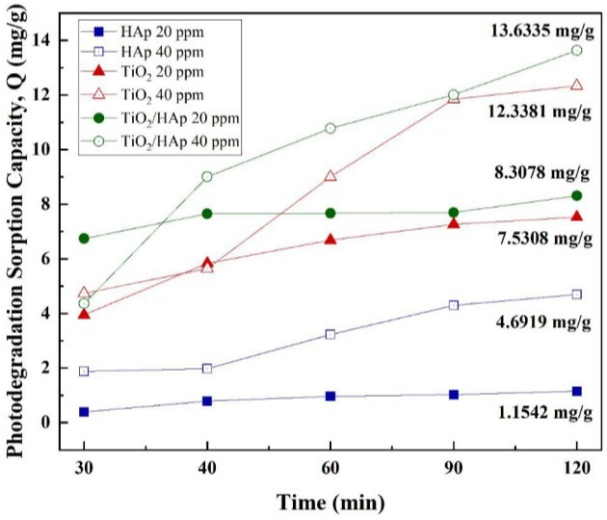

Figure 6. Absorption capacity in methylene blue photodegradation process

The absorption capacity in the adsorption process is also compared with the absorption capacity in the photodegradation process of methylene blue, as shown in Figure 6. Photodegradation conditions reduce the ability of HAp to absorb, indicating that HAp functions optimally under dark conditions (adsorption). The absorption capacity of TiO_2 in the photodegradation process increases compared to its absorption capacity in the adsorption process. During the photodegradation process, the photocatalytic capacity of TiO_2 is activated under UV light exposure, which leads to electron excitation from the valence band to the conduction band, generating electron-hole pairs [33]. In contrast, during the adsorption process under dark conditions, the photocatalytic activity is not activated.

The absorption capacity during the photodegradation process shows a more significant decrease in methylene blue concentration starting from the 40th minute for TiO_2/HAp compared to TiO_2 and HAp. This suggests that HAp plays a role in inhibiting the electron recombination process generated by TiO_2. The higher absorption capacity of TiO_2/HAp, compared to TiO_2 and HAp alone, supports this hypothesis.

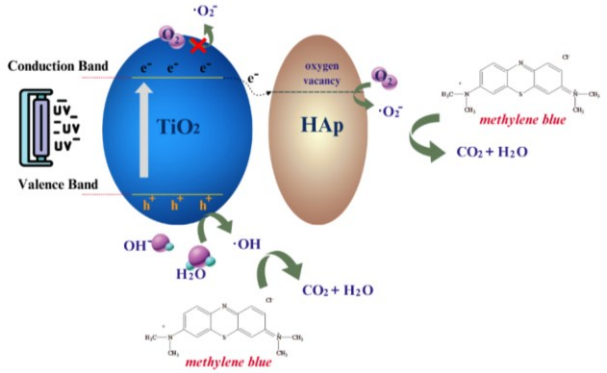

Figure 7. Photodegradation mechanism of methylene blue using TiO_2/HAp [9]

3.3.3. Degradation Mechanism of Methylene Blue by TiO_2/HAp Composite

Based on the analysis results, the photocatalytic mechanism of TiO_2/HAp under UV irradiation is illustrated in Figure 7. Upon UV exposure, TiO_2 photocatalysts generate electron-hole pairs, with electrons excited from the valence band to the conduction band. These electrons are transferred to the oxygen vacancy sites on the HAp surface [9]. Oxygen defects, which can form at elevated temperatures (~500–700°C), lead to the release of oxygen atoms from the PO_4 group, resulting in oxygen vacancies within the HAp structure [34].

The energy level at the oxygen defect sites on the HAp surface is lower than that of the TiO_2 conduction band, facilitating the transfer of excited electrons to HAp. These captured electrons then react with surrounding oxygen to form superoxide radicals (O_2^-). The electron transfer from TiO_2 to HAp helps to inhibit the recombination of the electron-hole pairs [9]. Simultaneously, holes in the TiO_2 valence band react with water (H_2O) to produce hydrogen ions (H^+) and hydroxyl radicals (OH). Both superoxide and hydroxyl radicals then interact with methylene blue molecules, degrading them into simpler compounds such as CO_2 and H_2O.

4. Conclusion

Based on the research results, it can be concluded that the TiO_2/HAp composite has been successfully synthesized, as evidenced by the XRD data, which show a combination of crystalline and amorphous peaks. FTIR spectra further confirm the presence of peaks corresponding to both TiO_2 and HAp. BET-BJH data indicate a decrease in surface area and pore volume for TiO_2/HAp compared to TiO_2, likely due to pore blockage. The TiO_2/HAp composite demonstrates high effectiveness in the photodegradation process. As the irradiation time increases, TiO_2/HAp shows higher degradation efficiency than TiO_2 and HAp, with photodegradation rates of 99.10% at 20 ppm and 86.47% at 40 ppm. The absorption capacity of TiO_2/HAp in the photodegradation process reaches 8.3078 mg/g at 20 ppm and 13.6335 mg/g at 40 ppm after 120 minutes. Therefore, the properties of HAp help inhibit electron recombination in TiO_2, thereby enhancing the photocatalytic performance.

Acknowledgment

The author would like to express sincere gratitude to all parties who contributed to the success of this research, particularly Dr. F. Widhi Mahatmanti, M.Si., for her invaluable financial support. The author also thanks to the Inorganic and Chemical Research Laboratory staff at Universitas Negeri Semarang for providing the necessary laboratory facilities.

References

[1] Vanitha Katheresan, Jibrail Kansedo, Sie Yon Lau, Efficiency of various recent wastewater dye removal methods: A review, *Journal of Environmental Chemical Engineering*, 6, 4, (2018), 4676-4697 https://doi.org/10.1016/j.jece.2018.06.060

[2] M. T. Hernández-Botello, S. B. Andrade-Canto, M. D. S. López-Cortez, D. E. Leyva-Daniel, Z. E. Delgado-Huerta, F. Garcia-Ochoa, Microscopy and Spectroscopy Analyses of Methylene Blue Biosorption on *Pennisetum clandestinum* Waste, *International Journal of Biological and Natural Sciences*, 2, 5, (2022), 2-11 https://doi.org/10.22533/at.ed.813252220073

[3] Jonathan O. Babalola, Babatunde A. Koiki, Yetunde Eniayewu, Abiola Salimonu, Joshua O. Olowoyo, Vincent O. Oninla, Helen A. Alabi, Augustine E. Ofomaja, Martins O. Omorogie, Adsorption efficacy of *Cedrela odorata* seed waste for dyes: Non linear fractal kinetics and non linear equilibrium studies, *Journal of Environmental Chemical Engineering*, 4, 3, (2016), 3527-3536 https://doi.org/10.1016/j.jece.2016.07.027

[4] Peter Olusakin Oladoye, Timothy Oladiran Ajiboye, Elizabeth Oyinkansola Omotola, Olusola Joel Oyewola, Methylene blue dye: Toxicity and potential elimination technology from wastewater, *Results in Engineering*, 16, (2022), 100678 https://doi.org/10.1016/j.rineng.2022.100678

[5] Khalil El Abbadi, Fatine Echabbi, Younes Ouzidan, Amina Khalidi-Idrissi, Rajae Lakhmiri, Mohamed Safi, The study on the use of a biocatalyst based on Calcined Cow Teeth-TiO_2 composite in degrading the methylene blue dye, *Results in Chemistry*, 6, (2023), 101027 https://doi.org/10.1016/j.rechem.2023.101027

[6] Sri Hilma Siregar, Prasetya Prasetya, Norramizawati Norramizawati, Marlian Marlian, Aulia Rizki Ramadhanti, Titanium Dioxide (TiO_2) Modified Bentonite for Photodegradation in Methylene Blue Dye, *Jurnal Kimia Sains dan Aplikasi*, 26, 4, (2023), 143-150 https://doi.org/10.14710/jksa.26.4.143-150

[7] Maria Sadia, Robina Naz, Jehangir Khan, Muhammad Zahoor, Riaz Ullah, Rizwan Khan, Sumaira Naz, Hesham S. Almoallim, Sulaiman Ali Alharbi, Metal doped titania nanoparticles as efficient photocatalyst for dyes degradation, *Journal of King Saud University - Science*, 33, 2, (2021), 101312 https://doi.org/10.1016/j.jksus.2020.101312

[8] Bruno C. B. Salgado, Antoninho Valentini, Evaluation of the Photocatalytic Activity of SiO_2@TiO_2 Hybrid Spheres in the Degradation of Methylene Blue and Hydroxylation of Benzene: Kinetic and Mechanistic Study, *Brazilian Journal of Chemical Engineering*, 36, 4, (2019), 1501-1518 http://dx.doi.org/10.1590/0104-6632.20190364s20190139

[9] Jie Yao, Yufei Zhang, Yawen Wang, Meijuan Chen, Yu Huang, Junji Cao, Wingkei Ho, Shun Cheng Lee, Enhanced photocatalytic removal of NO over titania/hydroxyapatite (TiO_2/HAp) composites with improved adsorption and charge mobility ability, *RSC Advances*, 7, 40, (2017), 24683-24689 https://doi.org/10.1039/C7RA02157G

[10] Qing Guo, Chuanyao Zhou, Zhibo Ma, Xueming Yang, Fundamentals of TiO_2 Photocatalysis: Concepts, Mechanisms, and Challenges, *Advanced Materials*, 31, 50, (2019), 1901997 https://doi.org/10.1002/adma.201901997

[11] M. Humayun, F. Raziq, A. Khan, W. Luo, Modification strategies of TiO_2 for potential applications in photocatalysis: a critical review, *Green Chemistry Letters and Reviews*, 11, 2, (2018), 86-102 https://doi.org/10.1080/17518253.2018.1440324

[12] Xuesong Zhao, Guan Zhang, Zhenghua Zhang, TiO_2-based catalysts for photocatalytic reduction of aqueous oxyanions: State-of-the-art and future prospects, *Environment International*, 136, (2020), 105453 https://doi.org/10.1016/j.envint.2019.105453

[13] Zhuang Zhang, Shuqin Zhang, Dajun Ren, Xiaoqing Zhang, Kan Tang, Xu Zhang, Adsorption characteristic of Cd^{2+} on the nano-hydroxyapatite/biochar hybrid materials derived from rice husk and eggshells, *Desalination and Water Treatment*, 287, (2023), 182-190 https://doi.org/10.5004/dwt.2023.29391

[14] Mashrafi Bin Mobarak, Nigar Sultana Pinky, Fariha Chowdhury, Md Sahadat Hossain, Monika Mahmud, Md Saiful Quddus, Shirin Akter Jahan, Samina Ahmed, Environmental remediation by hydroxyapatite: Solid state synthesis utilizing waste chicken eggshell and adsorption experiment with Congo red dye, *Journal of Saudi Chemical Society*, 27, 5, (2023), 101690 https://doi.org/10.1016/j.jscs.2023.101690

[15] Narendra Singh, Rajat Chakraborty, Raju Kumar Gupta, Mutton bone derived hydroxyapatite supported TiO_2 nanoparticles for sustainable photocatalytic applications, *Journal of Environmental Chemical Engineering*, 6, 1, (2018), 459-467 https://doi.org/10.1016/j.jece.2017.12.027

[16] F. Echabbi, M. Hamlich, S. Harkati, A. Jouali, S. Tahiri, S. Lazar, R. Lakhmiri, M. Safi, Photocatalytic degradation of methylene blue by the use of titanium-doped Calcined Mussel Shells CMS/TiO_2, *Journal of Environmental Chemical Engineering*, 7, 5, (2019), 103293 https://doi.org/10.1016/j.jece.2019.103293

[17] E. R. Muñoz-Sanchez, C. D. Arrieta-Gonzalez, A. Quinto-Hernandez, E. Garcia-Hernandez, J. Porcayo-Calderon, Synthesis of hydroxyapatite from eggshell and its electrochemical characterization as a coating on titanium, *International Journal of Electrochemical Science*, 18, 9, (2023), 100204 https://doi.org/10.1016/j.ijoes.2023.100204

[18] H. Bouyarmane, C. El Bekkali, J. Labrag, I. Es-saidi, O. Bouhnik, H. Abdelmoumen, A. Laghzizil, J. M. Nunzi, D. Robert, Photocatalytic degradation of emerging antibiotic pollutants in waters by TiO_2/Hydroxyapatite nanocomposite materials, *Surfaces and Interfaces*, 24, (2021), 101155 https://doi.org/10.1016/j.surfin.2021.101155

[19] I Nyoman Sukarta, I Dewa Ketut Sastrawidana, Synthesis and Characterization of Hydroxyapatite/Titania Composite and its Application on Photocatalytic Degradation of Remazol Red B Textile Dye under UV Irradiation, *Ecological Engineering & Environmental Technology*, 25, 2, (2024), 178-189 https://doi.org/10.12912/27197050/176230

[20] Md Sahadat Hossain, Shirin Akter Jahan, Samina Ahmed, Crystallographic characterization of bio-waste material originated $CaCO_3$, green-synthesized CaO and $Ca(OH)_2$, *Results in Chemistry*, 5, (2023), 100822 https://doi.org/10.1016/j.rechem.2023.100822

[21] Vinodhini Gopalakrishnan, Chandrasekaran Ramaswamy, Patient opinion mining to analyze drugs satisfaction using supervised learning, *Journal of Applied Research and Technology*, 15, 4, (2019), https://doi.org/10.1016/j.jart.2017.02.005

[22] Gullit Deffo, Mwina Basumatary, Nayab Hussain, Ranjit Hazarika, Shyamali Kalita, Evangéline Njanja, Panchanan Puzari, Eggshell nano-$CaCO_3$ decorated PANi/rGO composite for sensitive determination of ascorbic acid, dopamine, and uric acid in human blood serum and urine, *Materials Today Communications*, 33, (2022), 104357 https://doi.org/10.1016/j.mtcomm.2022.104357

[23] Reta G. Jalu, Tariku A. Chamada, Dr. Ramachandran Kasirajan, Calcium oxide nanoparticles synthesis from hen eggshells for removal of lead (Pb(II)) from aqueous solution, *Environmental Challenges*, 4, (2021), 100193 https://doi.org/10.1016/j.envc.2021.100193

[24] A. Prihanto, S. Muryanto, R. Ismail, J. Jamari, A. P. Bayuseno, Batch hydrothermal synthesis of nanocrystalline, thermostable hydroxyapatite at various pH and temperature levels, *Inorganic Chemistry Communications*, 157, (2023), 111301 https://doi.org/10.1016/j.inoche.2023.111301

[25] C. Vanitha, R. Abirami, S. Chandraleka, M. R. Kuppusamy, T. M. Sridhar, Green synthesis of photocatalyst hydroxyapatite doped TiO_2/GO ternary nanocomposites for removal of methylene blue dye, *Materials Today: Proceedings*, (2023), https://doi.org/10.1016/j.matpr.2023.02.354

[26] Md Sahadat Hossain, Samina Ahmed, Easy and green synthesis of TiO_2 (Anatase and Rutile): Estimation of crystallite size using Scherrer equation, Williamson-Hall plot, Monshi-Scherrer Model, size-strain plot, Halder- Wagner Model, *Results in Materials*, 20, (2023), 100492 https://doi.org/10.1016/j.rinma.2023.100492

[27] Bella Safitri, Heni Yohandini, Muharni Muharni, Salni Salni, Poedji Loekitowati Hariani, Synthesis of $NiFe_2O_4$ Magnetic Using *Artocarpus altilis* Leave Extract for Photocatalytic Degradation of Methylene Blue Dye and Antibacterial Applications, *Jurnal Kimia Sains dan Aplikasi*, 27, 8, (2024), 371-380 https://doi.org/10.14710/jksa.27.8.371-380

[28] Novesar Jamarun, Arika Prasejati, Zulhadjri Zulhadjri, Sintia Caniago, Tri Yupi Amirullah, Wulandari Wulandari, Vivi Sisca, Effect of chitosan concentration on hydroxyapatite/chitosan composite synthesis using the in-situ method as a dye adsorbent, *Kuwait Journal of Science*, 51, 4, (2024), 100252 https://doi.org/10.1016/j.kjs.2024.100252

[29] Muhammad Bilal, Javed Ali, Muhammad Umar, Sher Bahadar Khan, Adil Shaheen, Noushad Hussain, Rifat Jahan, Khan Malook, Mughal Qayum, Kalsoom Akhtar, Esraa M. Bakhsh, Ecofriendly synthesis of hydroxyapatite from fish scales and its application toward adsorptive removal of Pb(II), *Journal of the Indian Chemical Society*, 101, 8, (2024), 101175 https://doi.org/10.1016/j.jics.2024.101175

[30] Ramesh Vinayagam, Sandhya Kandati, Gokulakrishnan Murugesan, Louella Concepta Goveas, Aishwarya Baliga, Shraddha Pai, Thivaharan Varadavenkatesan, K. Kaviyarasu, Raja Selvaraj, Bioinspiration synthesis of hydroxyapatite nanoparticles using eggshells as a calcium source: Evaluation of Congo red dye adsorption potential, *Journal of Materials Research and Technology*, 22, (2023), 169-180 https://doi.org/10.1016/j.jmrt.2022.11.093

[31] Charlena Charlena, Akhiruddin Maddu, Tatang Hidayat, Synthesis and Characterization of Hydroxyapatite from Green Mussel Shell with Sol-Gel Method, *Jurnal Kimia Valensi*, 8, 2, (2022), 269-279 https://doi.org/10.15408/jkv.v8i2.27494

[32] Maocong Hu, Zhenhua Yao, Xuguang Liu, Liping Ma, Zhong He, Xianqin Wang, Enhancement mechanism of hydroxyapatite for photocatalytic degradation of gaseous formaldehyde over TiO_2/hydroxyapatite, *Journal of the Taiwan Institute of Chemical Engineers*, 85, (2018), 91-97 https://doi.org/10.1016/j.jtice.2017.12.021

[33] Yeganeh Kosar Hashemi, Mohammad Tavakkoli Yaraki, Sina Ghanbari, Leily Heidarpoor Saremi, Mohammad Hadi Givianrad, Photodegradation of organic water pollutants under visible light using anatase F, N co-doped TiO_2/SiO_2 nanocomposite: Semi-pilot plant experiment and density functional theory calculations, *Chemosphere*, 275, (2021), 129903 https://doi.org/10.1016/j.chemosphere.2021.129903

[34] Vladimir Bystrov, Ekaterina Paramonova, Leon Avakyan, José Coutinho, Natalia Bulina, Simulation and Computer Study of Structures and Physical Properties of Hydroxyapatite with Various Defects, *Nanomaterials*, 11, 10, (2021), 2752 https://doi.org/10.3390/nano11102752